Journal of Alloys and Compounds 509 (2011) 5190–5194

Contents lists available at ScienceDirect

Journal of Alloys and Compounds

journal homepage: www.elsevier.com/locate/jallcom

Microscopic origin of demixing in $Ge_{20}Se_xTe_{80-x}$ alloys

L. Rátkai[a], C. Conseil[b], V. Nazabal[b], B. Bureau[b], I. Kaban[c], J. Bednarcik[d], B. Beuneu[e], P. Jóvári[f,*]

[a] Eötvös University of Sciences, Graduate School of Physics, H-1518 Budapest POB 32 Hungary
[b] Equipe Verres et Céramiques, UMR-CNRS 6226, Sciences Chimiques, Université de Rennes 1, 35042 Rennes, France
[c] IFW Dresden, Institute for Complex Materials, POB 270116, D-01171, Dresden, Germany
[d] Deutsches Elektronen Synchrotron DESY, Notkestrasse 85, D-22603 Hamburg, Germany
[e] Laboratoire Léon Brillouin, CEA-Saclay 91191 Gif sur Yvette Cedex France
[f] Research Institute for Solid State Physics and Optics, H-1525 Budapest, POB 49, Hungary

ARTICLE INFO

Article history:
Received 25 October 2010
Received in revised form 1 February 2011
Accepted 4 February 2011
Available online 5 March 2011

Keywords:
Amorphous materials
Atomic scale structure
Neutron diffraction
X-ray diffraction
EXAFS
IR optics

ABSTRACT

The structure of $Ge_{20}Se_xTe_{80-x}$ ($x = 5$, 10, 15, 20) glasses has been investigated by X-ray and neutron diffraction as well as Ge and Se K-edge extended X-ray absorption fine structure (EXAFS) measurements. Experimental datasets have been fitted simultaneously by the reverse Monte Carlo simulation technique. It has been found that all components obey the 8-N rule. Se binds preferentially to Ge. At $x = 20$, experimental data can be fitted without Se–Te bonding, but Se–Se bonds appear, and the Te–Te coordination number starts to increase. These observations show that though Se and Te are completely miscible in the liquid and in the solid phases the presence of Ge induces nanoscale phase separation.

1. Introduction

Though selenium and tellurium are in the same group of the periodic table, their ability to form glasses is completely different. Selenide glasses are very common and stable against crystallisation, presenting large glass-forming domains, whereas tellurium alloys often need a very fast quenching such as splash cooling in order to be amorphous [1,2]. Tellurium alloys, especially those of the ternary system Ge–Sb–Te exhibit pronounced changes of optical and electrical properties occurring on reversible crystallization of amorphous thin layers. These glasses, particularly the $Ge_2Sb_2Te_5$ composition, deposited as active layers, are widely applied in the Digital Versatile Disk (DVD) technology [3,4]. Due to the essential technological interest, the structure and physical properties of these glasses have also been intensively investigated during the past decade [5–7]. According to a recent investigation Te-rich Te–Ge–Cu alloys are good candidates for obtaining high performance thermoelectric materials [8].

The transparency of the chalcogen based glasses is governed by multiphonon absorption involving several phonons which interact at once to produce vibrational modes absorbing in the far-infrared spectral domain. The position of the IR cut-off is determined by the atomic weight of the chalcogen and the bond strength of the glass network. Due to the tellurium weight, glasses exclusively based on this heavy element are very exciting materials for far infrared applications. Driven by the Darwin mission [9] of the European Space Agency (ESA) as well as a mid-infrared sensing technology [10–13], an active research is currently conducted on new compositions that could be drawn into optical fiber. Within this framework, it has been recently demonstrated that telluride glasses with high stability and favourable optical properties could be fabricated either by alloying with Ge and Sb [14], Ge and Ga [15], Ge and I [16] or Ge and As [17,18]. The Ge–Se–Te alloys have also been studied for their optical properties [19]. Since the substitution of tellurium with selenium results in the deterioration of optical properties (multiphonon absorption) only low Se-content glasses can be applied in IR optics. The impact of a small addition of Se to binary Ge–Te glasses has been recently investigated [20].

Though the $Ge_{20}Te_{80}$ binary compound is a poor glass former that can be vitrified only by very fast cooling, Te-rich ternary $Ge_{20}Se_xTe_{80-x}$ alloys possess much better glass forming ability and a broad supercooled liquid region (112 K for $x = 5$) [20]. Alloys with $40 < x < 60$ demix in the liquid state and it is not possible to obtain homogeneous glasses by classical melt quenching. Glass forming ability becomes excellent on the Se-rich side of the tie line. Due to the complexity of this system, little is known about the structural

* Corresponding author. Tel.: +36 1 392 25 89; fax: +36 1 392 25 89.
E-mail address: jovari@mail.kfki.hu (P. Jóvári).

0925-8388/$ – see front matter © 2011 Elsevier B.V. All rights reserved.
doi:10.1016/j.jallcom.2011.02.032

Table 1
Density of $Ge_{20}Se_xTe_{80-x}$ glasses.

	$Ge_{20}Se_5Te_{75}$	$Ge_{20}Se_{10}Te_{70}$	$Ge_{20}Se_{15}Te_{65}$	$Ge_{20}Se_{20}Te_{60}$
Density (g/cm^3)	5.48	5.41	5.35	5.28
Number density ($Å^{-3}$)	0.0289	0.0292	0.0295	0.0297

background of glass formation and demixing. The aim of the present study is to determine short range order parameters (coordination numbers, bond lengths) and find relation between changes in glass forming ability and short range order in Te-rich $Ge_{20}Se_xTe_{80-x}$ alloys. For this purpose we carried out X-ray diffraction, neutron diffraction and Ge and Se K-edge EXAFS measurements. Experimental datasets have been fitted simultaneously by the reverse Monte Carlo simulation technique [21] and partial pair correlation functions, coordination numbers and nearest neighbour distances have been obtained from the resulting atomic configurations.

2. Experimental

2.1. Sample preparation

$Ge_{20}Se_xTe_{80-x}$ glasses (with $x = 5$, 10, 15 and 20) were prepared by putting the high purity chemical reagents Te (5N), Se (5N) and Ge (5N) in the appropriate stoichiometry into a silica tube, which was then sealed under vacuum. For this structural study, the chemical reagents were not further purified before being introduced into the silica set-up. The ampoules with alloys were placed into a rocking furnace at 750 °C for typically 10 h. Then, the batch is homogenized at about 450 °C during 4 h before quenching in water, annealed at 150 °C (3 h) and, finally, cooled down slowly to the room temperature. The amorphous character of the glasses was checked by X-ray diffraction using a Philips PW3710 diffractometer operating with Cu Kα radiation ($\lambda = 1.5418$ Å).

2.2. Measurements

Density of the alloys was determined by the Archimedian technique, by measuring the weight of sample pieces in air and water. The estimated error of the density values (Table 1) is around ± 0.01 g/cm^3.

Neutron diffraction experiments were carried out at the 7C2 diffractometer (Laboratoire Léon Brillouin, CEA-Saclay). Samples were filled into vanadium containers (diameter 6 mm, wall thickness 0.1 mm). The wavelength of incident neutrons λ was 0.721 Å. Raw data were corrected for detector efficiency, background and incoherent scattering.

High-energy X-ray diffraction (XRD) measurements were performed at the BW5 experimental station [22] of the DORIS III positron storage ring (HASYLAB, Hamburg,). The energy of incident photons was 100 keV ($\lambda = 0.124$ Å). Powder samples were placed into thin walled (20 μm) quartz capillaries with outer diameter of 2 mm. The cross section of the incident beam was 1 mm × 1 mm. Scattered intensities were measured by a MAR345 imaging plate detector (2300 × 2300 pixels, with pixel size of 150 μm × 150 μm). Twenty measurements were carried out on each sample. Samples were illuminated for 20 s in each measurement. Comparison of scattered intensities did not reveal any radiation induced structural change. The sample-detector distance was 45 cm permitting a range of the diffraction vector $Q = 4\pi\sin(\theta)/\lambda$ (θ is half the scattering angle) up to ~18 Å^{-1}. The sample-to-detector distance and tilt of the imaging plate relative to the beam path were determined by measuring LaB_6 standard. Raw 2D intensity was corrected for background, and the result was integrated to Q-space using the software package FIT2D [23]. The Q-space intensity data were corrected for polarization, sample absorption, fluorescence, and Compton scattering using standard procedures described in [24]. X-ray and neutron diffraction structure factors are shown in Fig. 1.

Ge and Se K-edge EXAFS experiments were carried out at the beamline X of HASYLAB. Spectra were measured in transmission mode using fixed exit double-crystals Si(1 1 1) and Si(3 1 1). The intensities before and after the sample as well as after the reference samples were recorded by three ionization chambers filled with a mixture of Ar/Kr (~10% absorption), Ar (~50% absorption) and Kr (~100% absorption), respectively. The X-ray absorption cross sections μ(E) were converted to χ(k) by using the program VIPER [25]. Ge and Se K-edge χ(k) curves are shown in Fig. 1.

3. Reverse Monte Carlo simulation

Calculations were carried out with the new rmc++ code [26]. Simulation boxes usually contained 20,000 atoms. Minimum interatomic distances (cut-offs) for Ge–Ge, Ge–Se, Ge–Te, Se–Se, Se–Te and Te–Te pairs were usually 3.2 Å, 2.1 Å, 2.4 Å, 3.1 Å, 2.3 Å and 2.5 Å, respectively, excluding both Ge–Ge ($d_{Ge-Ge} \approx 2.45$ Å) and Se–Se ($d_{Se-Se} \approx 2.30$ Å) bonds for $5 \le x \le 15$. In case of $Ge_{20}Se_{20}Te_{60}$, Se–Se bonding had to be allowed to get a good fit of experimental datasets. On the other hand, for $Ge_{20}Se_5Te_{75}$ and $Ge_{20}Se_{20}Te_{60}$ the introduc-

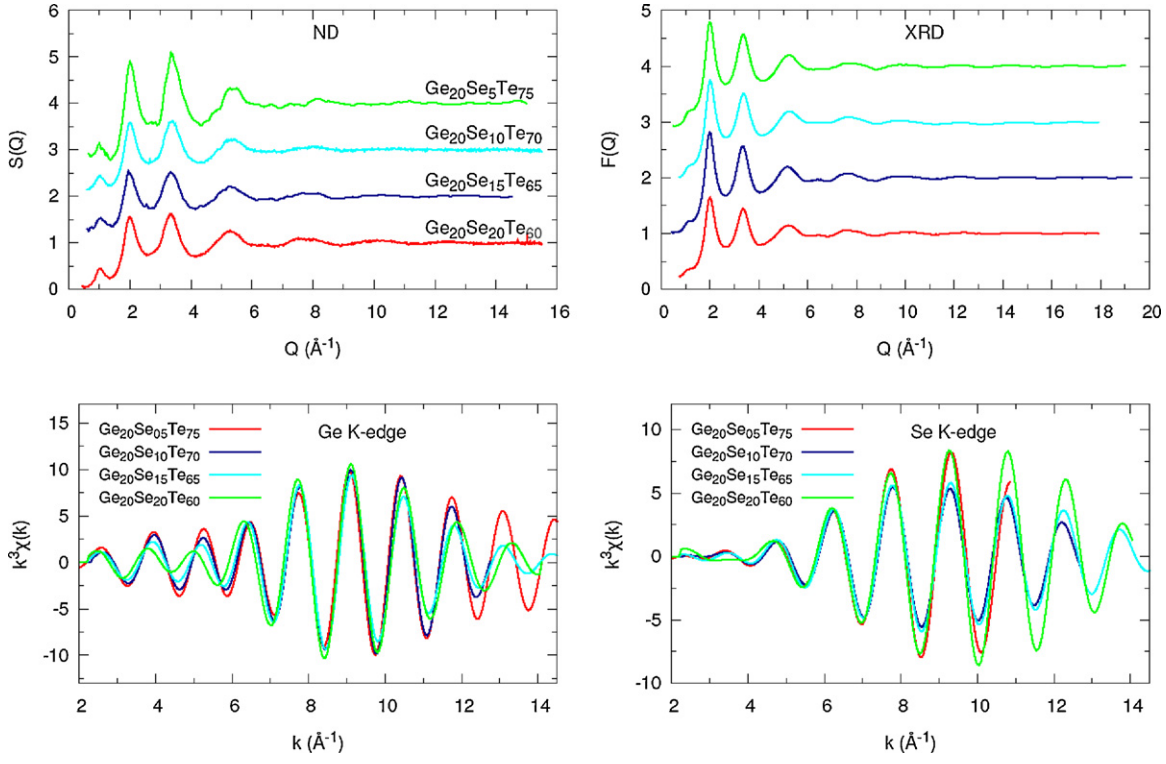

Fig. 1. X-ray- and neutron diffraction structure factors as well as Ge and Se K-edge EXAFS $k^3\chi(k)$ curves of $Ge_{20}Se_xTe_{80-x}$ glasses.

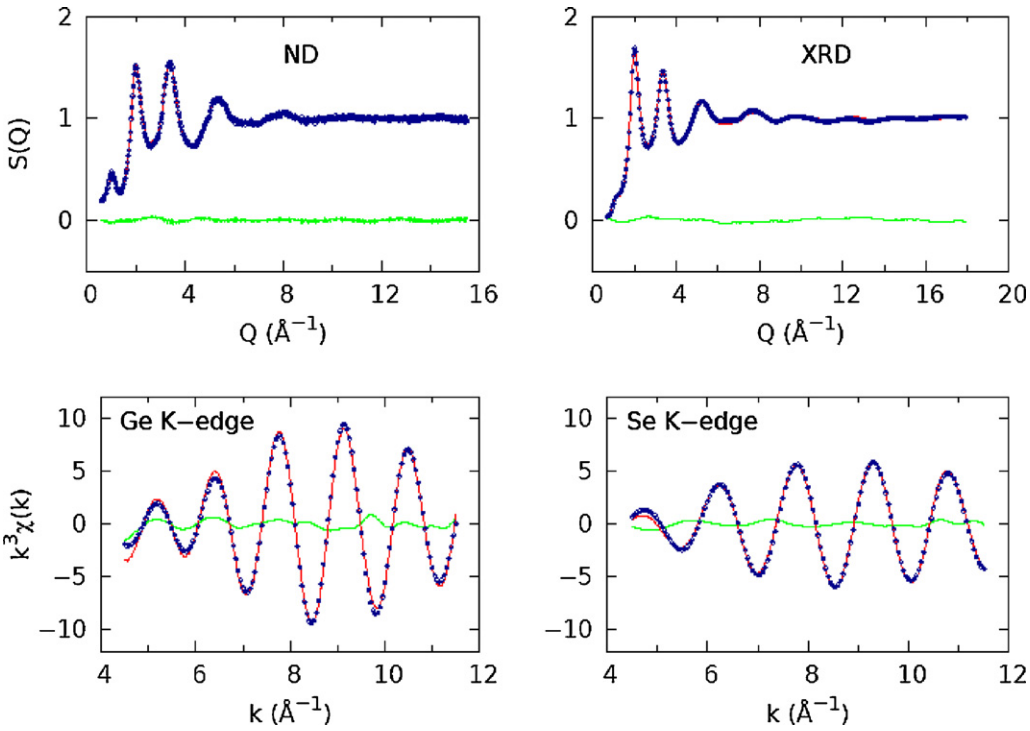

Fig. 2. Experimental data (dotted line), model curves (solid line) and their difference (green curves) obtained by the simultaneous fitting of X-ray- and neutron diffraction structure factors and Ge and Se K-edge EXAFS $k^3\chi(k)$ curves of $Ge_{20}Se_{15}Te_{65}$.

Table 2
Coordination numbers N_{ij} in $Ge_{20}Se_xTe_{80-x}$ glasses. Total coordination numbers of Ge and Se were constrained (see text for details).

	N_{GeSe}	N_{GeTe}	N_{SeGe}	N_{SeSe}	N_{SeTe}	N_{TeGe}	N_{TeSe}	N_{TeTe}	N_{Ge}	N_{Se}	N_{Te}
$Ge_{20}Se_5Te_{75}$	0.50	3.55	2.00	0.00	0.00	0.95	0.00	1.18	4.05	2.00	2.13
$Ge_{20}Se_{10}Te_{70}$	0.68	3.30	1.35	0.00	0.65	0.94	0.09	1.05	3.98	2.00	2.08
$Ge_{20}Se_{15}Te_{65}$	1.10	2.89	1.46	0.00	0.53	0.89	0.12	1.02	3.99	1.99	2.03
$Ge_{20}Se_{20}Te_{60}$	1.55	2.33	1.55	0.50	0.00	0.78	0.00	1.24	3.88	2.05	2.02

tion of Se–Te bonding did not improve the quality of the fits, and the corresponding cut-off could be raised to 3.1 Å. Besides cut-offs, coordination number constraints were also applied (see the next section). EXAFS spectra were fitted simultaneously with diffraction datasets. Backscattering factors needed to calculate model χ(k) curves from the partial pair correlation functions were calculated by the feff8.4 code [27]. For details of simultaneous fitting of EXAFS and diffraction measurements we refer to a recent paper [26]. Fig. 2 shows the typical quality of fits obtained by modelling simultaneously four experimental datasets.

4. Results and discussion

The structure of glassy $Ge_{15}Te_{85}$ was investigated recently by diffraction techniques and EXAFS [28]. Experimental data were fitted by reverse Monte Carlo simulation without using coordination constraints. It was found that the average coordination number of Ge is very close to 4 and the Ge–Ge coordination number is below the detection limit (~0.3). Thus it was concluded that the covalent network is built up of $GeTe_4$ tetrahedra linked to each other directly or via a bridging Te atom. On the basis of this previous work, it is reasonable to assume that Ge is fourfold coordinated in $Ge_{20}Te_{80}$ and $Ge_{20}Se_xTe_{80-x}$ alloys as well. For this reason each Ge atom was forced to have 4 neighbours (Se or Te) in the models. Se atoms had to have 2 neighbours (Ge or Te for $x = 10$, 15, Ge for $x = 5$ and Ge or Se for $x = 20$). On the other hand, no such coordination constraint was applied to Te atoms. The reason for this extra freedom is that in some glasses the coordination number of Te does not obey the 8-N rule [29]. For example in $Ga_{11}Ge_{11}Te_{78}$ the average coordination number of Te was 2.39 ± 0.2 [28]

Partial pair correlation functions are shown in Fig. 3 while coordination numbers and nearest neighbour distances are given in Table 2 and Table 3. It can be observed that N_{Te}, the coordination number of Te is close to 2 over the whole concentration range investigated. As N_{Te} was not constrained, the above result strongly suggests that the 8-*N* rule is valid for Te in $Ge_{20}Se_xTe_{80-x}$ glasses as well. The average number of Ge atoms around a Te atom, N_{TeGe}, is close to 1 for $x = 5$ (0.95 ± 0.15) meaning that the structure is mainly built up of $GeTe_4$ tetrahedra connected by Te–Te dimers. On the other hand, $N_{SeGe} = 2.0$ shows that selenium atoms directly bridge tetrahedra centred on Ge. We note here that Se–Te bonding in $Ge_{20}Se_5Te_{75}$ was tested by decreasing the minimum Se–Te distance to 2.3 Å. Fit quality did not improve, the resulting coordination number (0.29) was just around the detection limit and the Se–Te bond length was around 2.70 Å. This value is much longer than the Se–Te distance (~2.60 Å) found either in other $Ge_{20}Se_xTe_{80-x}$

Table 3
Nearest neighbour distances r_{ij} (in Å) and in $Ge_{20}Se_xTe_{80-x}$ glasses. The uncertainty of r_{ij} values is around 0.02 Å.

	r_{GeSe}	r_{GeTe}	r_{SeSe}	r_{SeTe}	r_{TeTe}
$Ge_{20}Se_5Te_{75}$	2.36	2.60	–	–	2.74
$Ge_{20}Se_{10}Te_{70}$	2.35	2.60	–	2.60	2.73
$Ge_{20}Se_{15}Te_{65}$	2.37	2.59	–	2.60	2.71
$Ge_{20}Se_{20}Te_{60}$	2.38	2.62	2.30	–	2.71

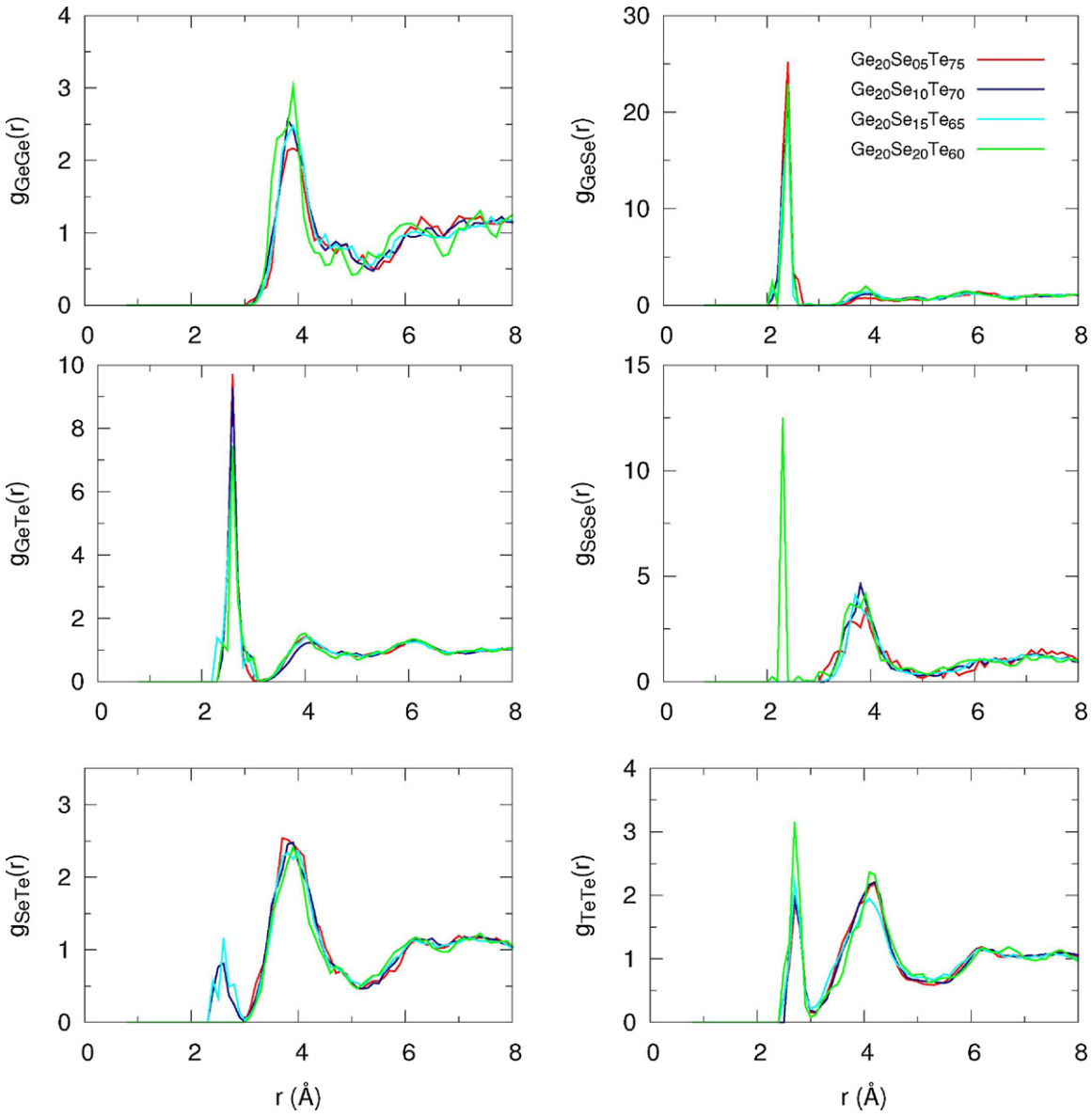

Fig. 3. Partial pair correlation functions of $Ge_{20}Se_xTe_{80-x}$ glasses obtained by reverse Monte Carlo simulation of diffraction and EXAFS datasets.

glasses or in vitreous $As_3Se_5Te_2$ [30]. Therefore, we believe that at low concentrations Se binds predominantly to Ge. N_{TeGe} decreases to 0.89 ± 0.15 for $x = 15$ to the benefit of N_{TeSe} which increases to 0.12 in agreement with substitution of Se to Te in the dimers. Up to $x = 15$, Ge is replaced by Se around Te atoms. As a result, the sum of N_{TeGe} and N_{TeSe} is equal to 1 (within the uncertainty of modelling). At $x = 20$, N_{TeSe} (and N_{SeTe}) drops to zero and N_{TeTe} increases to 1.24 ± 0.15. 'Zero' means here that the Se–Te cut-off can be increased to 3.1 without changing fit quality. Another important feature is the appearance of Se–Se bonds ($N_{SeSe} = 0.50 \pm 0.3$). It is noteworthy that without Se–Se bonding the *R*-factor of the fit of Se K-edge EXAFS data was 290% higher. The *R*-factor in the rmc++ programme is defined by the following equation:

$$R = \frac{\sqrt{\sum (\chi_{calc} - \chi_{exp})^2}}{\sqrt{\sum \chi_{exp}^2}} \quad (1)$$

where χ_{calc} and χ_{exp} are the calculated and experimental EXAFS curves and summations run over all experimental points.

Since Te–Se coordination numbers are rather low, dedicated test runs were carried out to judge their significance in $Ge_{20}Se_{10}Te_{70}$ and $Ge_{20}Se_{15}Te_{65}$. In these runs, the average Te–Se coordination number was changed (by steps of ±0.3) using appropriate constraints and the resulting *R*-factors were compared. It was found that Te–Se bonding is necessary to get reasonable fit of Se K-edge EXAFS data in the case of $Ge_{20}Se_{10}Te_{70}$. For this alloy, the *R*-factor of Se EXAFS fit increased with 70% upon eliminating Te–Se bonding. For $Ge_{20}Se_{15}Te_{65}$ the corresponding change was much smaller (~12%) which strongly questions Te–Se bonding in this composition. Nevertheless, the mean Se–Te distance r_{SeTe} is 2.60 Å, which is equal to the Se–Te distance found in $Ge_{20}Se_{10}Te_{70}$ and in glassy $As_3Se_5Te_2$ [30]. For this reason, we believe that Se–Te bonding does not vanish in $Ge_{20}Se_{15}Te_{65}$.

Our results clearly indicate that at around $x = 20$ the number of Se–Se and Te–Te bonds start to increase which may be regarded as the first step towards demixing. Se and Te are completely miscible in each other in the liquid as well as in the solid state where they form an isomorphous system [31]. Therefore demixing should be caused by the difference of Ge–Se and Ge–Te interactions. At

$x = 5$, N_{GeSe} is 0.50 ± 0.2 and N_{GeTe} is 3.55 ± 0.2. Both N_{GeSe} and N_{GeTe} change monotonically with Se concentration. At $x = 20$ N_{GeSe} is as high as 1.55 ± 0.2, while N_{GeTe} is equal to 2.33 ± 0.2. If Se and Te could replace each other in a completely random way in $Ge_{20}Se_xTe_{80-x}$ glasses then N_{GeSe} (N_{GeTe}) should be proportional to the concentration of Se (Te) atoms and N_{GeTe}/N_{GeSe} should be equal to c_{Te}/c_{Se}. In the case of $Ge_{20}Se_{20}Te_{60}$, N_{GeTe}/N_{GeSe} is $\sim 1.5 \pm 0.4$ while c_{Te}/c_{Se} is 3 which indicates that Ge strongly prefer Se to Te. This result has to be correlated with the infrared transmission of these glasses. It extends up to 20 μm for pure tellurium $GeTe_4$ composition and is reduced to about 18 μm for $Ge_{20}Se_xTe_{80-x}$ because of the Ge–Se bonds which give rise to a multi-phonon vibrational absorption band located at 19 μm.

Ge–Te nearest neighbour distances (2.59–2.62 Å, Table 3) agree well with the values found in $Ge_2Sb_2Te_5$ [32], $Ge_{15}Te_{85}$ and $Ge_{20}I_7Te_{73}$ [28]. The Ge–Se bond length is 2.35–2.38 Å, while the Ge–Se distance in glassy $GeSe_2$ and glassy $GeSe_4$ was found to be 2.37 Å in recent works [33,34]. Plausible values of the bond lengths together with the good quality of the fit (Fig. 2) show that our models are realistic and the partial pair correlation functions can be reliably separated by fitting four datasets simultaneously and using reasonable coordination constraints.

5. Conclusions

The structure of $Ge_{20}Se_xTe_{80-x}$ ($x = 5, 10, 15, 20$) alloys has been investigated by X-ray and neutron diffraction as well as extended X-ray fine structure (EXAFS) measurements. Experimental datasets have been fitted simultaneously by the reverse Monte Carlo simulation technique. The first noteworthy result is that in alloys with lower Se concentration the structure can be described as essentially built up of $GeTe_4$ tetrahedra connected to each other by Te–Te dimers. Se preferentially binds to Ge for all compositions investigated. For $x \leq 15$, the fits of experimental data are not improved by allowing Se-Se bonds. On the other hand, at $x = 20$ Se–Se bonds had to be considered to give a good account for the experiments. Simultaneously, experimental data can be fitted without Se–Te bonding and the Te–Te coordination starts to increase. These observations may be regarded as the first step towards demixing and show that Se and Te try to avoid each other in the presence of Ge which leads to a nanoscale phase separation.

Acknowledgments

P. Jóvári was supported by the Bolyai Research Fellowship of the Hungarian Academy of Sciences. The neutron diffraction measurement at LLB (CEA-Saclay, France) was supported by the European Commission under the 6th Framework Programme through the Key Action: Strengthening the European Research Area, Research Infrastructures. Contract No: HII3-CT-2003-505925.

References

[1] V.F. Kokorina, Glasses for Infrared Optics, in: Laser and Optical Science and Technology Series, CRC Press, 1996.
[2] B. Bureau, S. Danto, H.L. Ma, C. Boussard-Plédel, X.H. Zhang, J. Lucas, Solid State Sci. 10 (2008) 427–433.
[3] G.F. Zhou, Mater. Sci. Eng. A304–306 (2001) 73–80.
[4] B.S. Lee, J.R. Abelson, S.G. Bishop, D.H. Kang, B.K. Cheong, K.B. Kim, J. Appl. Phys. 97 (2005) 093509.
[5] P. Němec, A. Moreac, V. Nazabal, M. Pavlišta, J. Přikryl, M. Frumar, J. Appl. Phys. 106 (2009) 103509.
[6] S. Raoux, W. Welnic, D. Ielmini, Chem. Rev. 110 (2010) 240–267.
[7] M. Wuttig, N. Yamada, Nat. Mater. 6 (2007) 824–832.
[8] A.P. Gonçalves, E.B. Lopes, O. Rouleau, C. Godart, J. Mater. Chem. 20 (2010) 1516–1521.
[9] P. Houizot, C. Boussard-Plédel, A.J. Faber, L.K. Cheng, B. Bureau, P.A. Van Nijnatten, W.L.M. Gielesen, J. Pereira do Carmo, J. Lucas, Optics Exp. 15 (2007) 12529.
[10] C. Vigreux-Bercovici, E. Bonhomme, A. Pradel, J.E. Broquin, L. Labadie, P. Kern, Appl. Phys. Lett. 90 (2007) 011110.
[11] P. Lucas, M. Solis, D. LeCoq, C. Junker, M. Riley, J. Collier, D. Boesewetter, C. Boussard, B. Bureau, Sens. Actuators B 119 (2006) 355–362.
[12] X.H. Zhang, B. Bureau, C. Boussard, H.L. Ma, J. Lucas, Chemistry 14 (2008) 432–442.
[13] D. Le Coq, K. Michel, J. Keirsse, C. Boussard-Plédel, G. Fonteneau, B. Bureau, J.M. Le Quéré, O. Sire, J. Lucas, C.R. Chim. 5 (2002) 907–913.
[14] T. Katsuyama, H. Matsumura, J. Non-Cryst. Solids 139 (1992) 177–178.
[15] S. Danto, P. Houizot, C. Boussard-Plédel, X.H. Zhang, F. Smektala, J. Lucas, Adv. Funct. Mater. 16 (2006) 1847–1852.
[16] A. Wilhelm, C. Boussard-Plédel, Q. Coulombier, J. Lucas, B. Bureau, P. Lucas, Adv. Mater. 19 (2007) 3796–3800.
[17] Z.Y. Yang, P. Lucas, J. Am. Ceram. Soc. 92 (2009) 2920–2923.
[18] C. Vigreux-Bercovici, E. Bonhomme, A. Pradel, J. Non-Cryst. Solids 353 (2007) 1388–1391.
[19] T. Katsuyama, H. Matsumura, J. Appl. Phys. 76 (1994) 2036–2040.
[20] S. Maurugeon, B. Bureau, C. Boussard-Plédel, A.J. Faber, X.H. Zhang, W. Geliesen, J. Lucas, J. Non-Cryst. Solids 355 (2009) 2074–2078.
[21] R.L. McGreevy, L. Pusztai, Mol. Simul. 1 (1988) 359–367.
[22] R. Bouchard, D. Hupfeld, T. Lippmann, J. Neuefeind, H.B. Neumann, H.F. Poulsen, U. Rütt, T. Schmidt, J.R. Schneider, J. Süssenbach, M. von Zimmermann, J. Synchrotron Radiat. 5 (1998) 90–101.
[23] A.P. Hammersley, S.O. Svensson, M. Hanfland, A.N. Fitch, D. Häusermann, High Pressure Res. 14 (1996) 235–248.
[24] T. Egami, S.J.L. Billinge, Underneath the Bragg Peaks: Structural Analysis of Complex Materials, Pergamon Press, Elsevier, Oxford, England, 2003.
[25] K.V. Klementev, J. Phys. D: Appl. Phys. 34 (2001) 209–217.
[26] O. Gereben, P. Jóvári, L. Temleitner, L. Pusztai, J. Optoelectron. Adv. Mater. 9 (2007) 3021–3027.
[27] A.L. Ankudinov, B. Ravel, J.J. Rehr, S.D. Conradson, Phys. Rev. B 58 (1998) 7565–7576.
[28] P. Jóvári, I. Kaban, B. Bureau, A. Wilhelm, P. Lucas, B. Beuneu, D.A. Zajac, J. Phys. Condens. Matter 22 (2010) 404207.
[29] N. Mott, Adv. Phys. 16 (1967) 49–144.
[30] P. Jóvári, B. Bureau, I. Kaban, V. Nazabal, B. Beuneu, U. Rütt, J. Alloys Compd. 488 (2009) 39–43.
[31] T.B. Massalski, J.L. Murray, K.H. Bennet, H. Baker (Eds.), Binary Alloy Phase Diagrams, American Society for Metals, Metals Park, OH, 1986.
[32] P. Jóvári, I. Kaban, J. Steiner, B. Beuneu, A. Schöps, M.A. Webb, Phys. Rev. B 77 (2008) 035202.
[33] V. Petkov, D. Le Messurier, J. Phys.: Condens. Matter 22 (2010) 115402.
[34] I. Kaban, P. Jóvári, T. Petkova, P. Petkov, A. Stoilova, W. Hoyer, B. Beuneu, J. Phys. Condens. Matter 22 (2010) 404205.